ELSEVIER

Contents lists available at ScienceDirect

# Journal of Hydrology

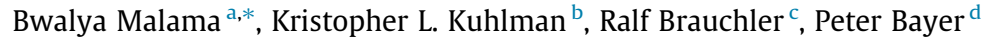
journal homepage: www.elsevier.com/locate/jhydrol

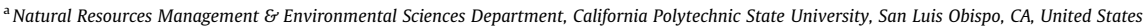


CrossMark

#### Research papers

## Modeling cross-hole slug tests in an unconfined aquifer





<sup>&</sup>lt;sup>b</sup> Sandia National Laboratories, Albuquerque, NM, United States

#### ARTICLE INFO

Article history:
Received 1 March 2016
Received in revised form 15 June 2016
Accepted 27 June 2016
Available online 28 June 2016
This manuscript was handled by P.
Kitanidis, Editor-in-Chief, with the assistance of Hund-Der Yeh, Associate Editor

Keywords: Cross-hole slug tests Multi-level Unconfined aquifer Hydraulic conductivity Specific storage Specific yield

#### ABSTRACT

A modified version of a published slug test model for unconfined aquifers is applied to cross-hole slug test data collected in field tests conducted at the Widen site in Switzerland. The model accounts for water-table effects using the linearized kinematic condition. The model also accounts for inertial effects in source and observation wells. The primary objective of this work is to demonstrate applicability of this semi-analytical model to multi-well and multi-level pneumatic slug tests. The pneumatic perturbation was applied at discrete intervals in a source well and monitored at discrete vertical intervals in observation wells. The source and observation well pairs were separated by distances of up to 4 m. The analysis yielded vertical profiles of hydraulic conductivity, specific storage, and specific yield at observation well locations. The hydraulic parameter estimates are compared to results from prior pumping and single-well slug tests conducted at the site, as well as to estimates from particle size analyses of sediment collected from boreholes during well installation. The results are in general agreement with results from prior tests and are indicative of a sand and gravel aquifer. Sensitivity analysis show that model identification of specific yield is strongest at late-time. However, the usefulness of late-time data is limited due to the low signal-to-noise ratios.

© 2016 Elsevier B.V. All rights reserved.

#### 1. Introduction

Slug tests are a common tool in hydrogeology for hydraulic characterization of aquifers because they are quick, obviate the need for waste water disposal, require less equipment, and are not as labor intensive as pumping tests. Fundamentally, they involve instantaneous (step) perturbation of fluid pressure in an interval followed by continuous monitoring of the pressure change as it dissipates by fluid flow through the aquifer. This is typically achieved by either dropping a slug mass into a well (Cooper et al., 1967) or pneumatically pressurizing the water column in a well (Butler, 1998; Malama et al., 2011), a configuration referred to as a single well test. Several mathematical models are available in the hydrogeology literature for analyzing confined (Cooper et al., 1967; Bredehoeft and Papadopulos, 1980; Zurbuchen et al., 2002; Butler and Zhan, 2004) and unconfined (Bouwer and Rice, 1976; Springer and Gelhar, 1991; Hyder et al., 1994; Spane, 1996; Zlotnik and McGuire, 1998; Malama et al., 2011) aquifer slug test data under the Darcian flow regime. Consideration of slug tests

under non-Darcian flow regimes may be found in Quinn et al. (2013) and Wang et al. (2015).

Slug tests have the advantage of only involving limited contact with and minimal disposal of effluent formation water. As such, they have found wide application for characterizing heterogeneous formations at contaminated sites (Shapiro and Hsieh, 1998) and for investigating flow in fractured rock (Quinn et al., 2013; Ji and Koh, 2015; Ostendorf et al., 2015). However, the small volumes of water involved impose a physical limit on the volume of the formation interrogated during tests (Shapiro and Hsieh, 1998; Beckie and Harvey, 2002) because the resulting pressure perturbations often do not propagate far enough to be measurable in observation wells. As a result, hydraulic parameters estimated from single well slugtest data can only be associated with the formation volume within the immediate vicinity of the source well (Beckie and Harvey, 2002; Butler, 2005).

Cross-hole (or multi-well) slug tests are less common but have been applied to interrogate relatively large formation volumes in what has come to be known as hydraulic tomography (Yeh and Liu, 2000; Illman et al., 2009). For example, Vesselinov et al. (2001) and Illman and Neuman (2001) used pneumatic cross-hole injection tests to hydraulically characterized a fractured

<sup>&</sup>lt;sup>c</sup> AF-Consult Switzerland Ltd, Baden, Switzerland

d ETH Zürich, Zürich, Switzerland

<sup>\*</sup> Corresponding author.

E-mail address: bmalama@scalpoly.edu (B. Malama).

#### Nomenclature finite Hankel transform parameter [-] characteristic length for source/observation well oscilla- $L_e/L_{e,obs}$ В aguifer initial thickness [L] tory term [L] length of source well test interval [L] Laplace transform parameter [-] bs р coefficient of wellbore storage [L<sup>2</sup>] radial coordinate, out from center of source well [L] $C_{w}$ r $d/d_0$ depth of top of source/observation well test interval be-R domain radius, out from center of source well [L] low watertable [L] radius of source well tubing at water-table [L] $r_c$ acceleration due to gravity $[LT^{-2}]$ $r_w$ radius of source well at test interval [L] hydraulic head change from equilibrium position in hydraulic head change from initial conditions [L] Н source well [L] $S_s$ specific storage [L<sup>-1</sup>] $H_0$ initial slug input [L] $S_y$ specific yield [-] Κ formation hydraulic conductivity [L T<sup>-1</sup>] time since slug initiation [T] radial formation hydraulic conductivity [LT<sup>-1</sup>] characteristic time ( $T_c = \dot{B}^2/\alpha_{r,1}$ ) [T] $T_c$ $K_r$ vertical coordinate, down from water-table [L] vertical formation hydraulic conductivity [LT<sup>-1</sup>] $K_z$ z hydraulic diffusivity of $i^{th}$ zone [L<sup>2</sup> T<sup>-1</sup>] skin hydraulic conductivity [L T<sup>-1</sup>] $K_{\rm skin}$ $\alpha_{r,i}$ $l/l_{o}$ depth of bottom of source/observation well test interval source well damping coefficient [T<sup>-1</sup>] $\gamma_s$ kinematic viscosity of water $[L^2 T^{-1}]$ below watertable [L] characteristic length for source/observation well damp- $L/L_{obs}$ ing term [L]

unsaturated rock formation with dimensions of  $30 \times 30 \times 30 \text{ m}^3$ . Barker and Black (1983) presented evidence of measurable pressure responses in observation wells several meters from the source well, Audouin and Bodin (2008) reported cross-hole slug tests conducted in fractured rock, where they collected data in observations wells at radial distances 30 to about 120 m from the source well. and observed maximum peak amplitudes ranging from 5 to 20 cm. This demonstrated empirically that slug test pressure perturbations can propagate over relatively large distances beyond the immediate vicinity of the source well, albeit for fractured rocks, which have high hydraulic diffusivities. Brauchler et al. (2010) attempted to intensively apply cross-hole slug tests to obtained a detailed image of confined aquifer heterogeneity. They used the model of Butler and Zhan (2004) to estimate aguifer hydraulic conductivity, specific storage and anisotropy. Cross-hole slug tests in unconfined aquifers, neglecting wellbore inertial effects, have been reported by Spane (1996), Spane et al. (1996), and Belitz and Dripps (1999) for source-to-observation well distances not exceeding 15 m.

Recently Paradis and Lefebvre (2013) and Paradis et al. (2014, 2015) analyzed synthetic cross-hole slug test data using a model for over-damped observation well responses. The need, therefore, still exists to analyze field data and characterize high permeability heterogeneous unconfined aquifers using cross-hole slug tests where source and observation well inertial effects may not be neglected. Malama et al. (2011) developed a slug test model for unconfined aguifers using the linearized kinematic condition of Neuman (1972) at the water-table, and accounting for inertial effects of the source well. They analyzed data from single-well tests performed in a shallow unconfined aguifer. This work extends the application of the model of Malama et al. (2011) to multi-well tests and to response data collected in observation wells. The data analyzed were collected at multiple vertical intervals in an observation well about 4 m from the source well, which itself was perturbed at multiple intervals. The model and data are used to estimate hydraulic conductivity, specific storage, and specific yield. The sensitivity of predicted model behavior to these parameters is also analyzed. In the following, the mathematical model is presented, the multi-level multi-well tests are described, and data analyzed. The work concludes with an analysis of the sensitivity coefficients for the hydraulic and well characteristic parameters.

#### 2. Slug test model

Malama et al. (2011) developed a model for formation and source well response to slug tests performed in unconfined aquifers using the linearized kinematic condition at the water-table. The model allows for estimation of specific yield in addition to hydraulic conductivity and specific storage. The model also accounts for source-well wellbore storage and inertial effects. Wellbore storage in the source well is treated in the manner of Cooper et al. (1967). A schematic of the conceptual model used to derive the semi-analytical solution is shown in Fig. 1. Whereas the solution of (Malama et al., 2011) was obtained for and applied to source wells, here a more complete solution is presented that applies to observation wells. The complete aquifer response for both source and observation wells is given by (see Appendix A and Malama et al. (2011) for details)

$$\hat{\overline{s}}_{D} = \hat{\overline{u}}_{D} \begin{cases}
\left[1 - \hat{\overline{v}}_{D}(d_{D})\right] \hat{\overline{f}}_{1}(z_{D}) & \forall z_{D} \in [0, d_{D}] \\
1 - \hat{\overline{v}}_{D} & \forall z_{D} \in [d_{D}, l_{D}] \\
\left[1 - \hat{\overline{v}}_{D}(l_{D})\right] \hat{\overline{f}}_{2}(z_{D}) & \forall z_{D} \in [l_{D}, 1],
\end{cases}$$
(1)

where  $\hat{s}_D$  is the double Laplace-Hankel transform of the dimensionless formation head response  $s_D = s/H_0$ ,  $d_D = d/B$  and  $l_D = l/B$  are dimensionless depths to the top and bottom of the test interval,  $z_D = z/B$  ( $z \in [0,B]$ ) is dimensionless depth below the water-table, B is initial saturated thickness,

$$\hat{\overline{u}}_D = \frac{C_D \left(1 - p\overline{H}_D\right)}{\kappa \eta^2 \xi_w K_1(\xi_w)},\tag{2}$$

$$\hat{\overline{\nu}}_D = \frac{\Delta_0(d_D)}{\Delta_0(1)} \cosh\left(\eta z_D^*\right) + \sinh\left(\eta_D^*\right) \frac{\Delta_0'(z_D)}{\eta \Delta_0(1)},\tag{3}$$

$$\hat{\bar{f}}_1(z_D) = \frac{d'_0(z_D)}{d'_0(d_D)},\tag{4}$$

$$\hat{\bar{f}}_2(z_D) = \frac{\cosh\left(\eta z_D^*\right)}{\cosh\left(\eta l_D^*\right)},\tag{5}$$

$$\Delta_0(z_D) = \sinh(\eta z_D) + \varepsilon \cosh(\eta z_D), \tag{6}$$

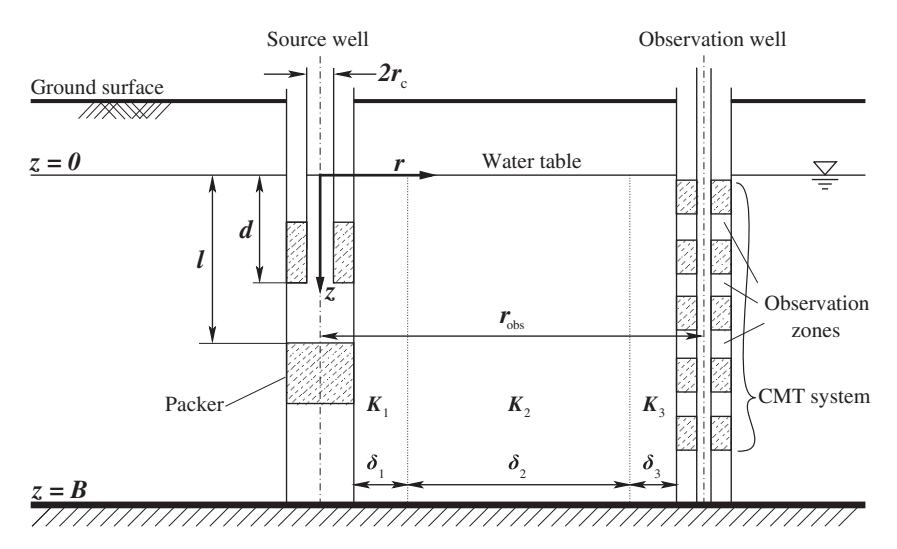


Fig. 1. Schematic of a typical cross-hole slug test set-up for an unconfined aquifer. For the tests reported herein, the source and observation intervals were isolated with a multi chamber well not a multi-packer system.

and

$$\Delta'_{0}(z_{D}) = \eta[\cosh(\eta z_{D}) + \varepsilon \sinh(\eta z_{D})]. \tag{7}$$

Additionally,  $z_D^*=1-z_D$ ,  $l_D^*=1-l_D$ ,  $\eta=\sqrt{(p+a_i^2)/\kappa}$ , p and  $a_i$  are the dimensionless Laplace and finite Hankel transform parameters,  $C_D=r_{D,c}^2/(b_sS_s)$  is the dimensionless wellbore storage coefficient of the source well,  $S_s$  is formation specific (elastic) storage,  $b_s=l-d$  the length of the source well completion interval,  $\kappa=K_z/K_r$  is the formation anisotropy ratio,  $K_z$  and  $K_r$  are vertical and radial hydraulic conductivities,  $\xi_W=r_{D,W}\sqrt{p}$ ,  $\varepsilon=p/(\eta\alpha_D)$ , and  $K_1()$  is the first-order second-kind modified Bessel function (Olver et al., 2010, Section 10.25). The relevant dimensionless parameters are listed in Table 1.

The function  $\overline{H}_D(p)$  in (2) is the Laplace transform of  $H_D(t_D)=H(t)/H_0$ , the normalized response in the source well, and is given by

**Table 1** Dimensionless variables and parameters.

```
s_{D,i} = s_i/H_0
H_D = H(t)/H_0
r_D = r/B
r_{D,w} = r_w/B
r_{D,c} = r_c/B
r_{D,s}=r_s/B
R_D = R/B
z_D = z/B
d_D = d/B
t_D = \alpha_{r,1} t/B^2
C_D = r_{D.c}^2/(bS_s)
\alpha_D = \kappa \sigma
\beta_1 = 8vL/\left(r_c^2gT_c\right)
\beta_2 = L_e / (gT_c^2)
\beta_{\rm D} = \beta_1/\sqrt{\beta_2}
\kappa_i = K_{z,i}/K_{r,i}
\sigma = BS_s/S_v
\gamma = K_{r,2}/K_{r,1}
\vartheta = 2bS_{s,2}(r_w/r_c)^2
\xi_{\rm sk} = r_{\rm sk}/r_{\rm w}
\xi_w = r_{D,w} \sqrt{p}
\eta^2 = (p + a_i^2)/\kappa
```

$$\overline{H}_{D}(p) = \frac{\overline{\psi}_{1}(p)}{\omega_{Ds}^{2} + p\overline{\psi}_{1}(p)},$$
(8)

where  $\omega_{D,s}=\omega_s T_c, \omega_s=\sqrt{g/L_e}$  is the source well frequency,  $L_e$  is a characteristic length associated with the source well oscillatory term,  $T_c=B^2/\alpha_r$  is a characteristic time, g is the acceleration due to gravity, and

$$\overline{\psi}_1(p) = p + \gamma_{D,s} + \frac{\omega_{D,s}^2}{2} \overline{\Omega}(r_{D,w}, p). \tag{9}$$

The function  $\overline{\Omega}$  is defined by

$$\overline{\Omega}(r_{D,w},p) = \mathsf{H}_0^{-1} \left\{ \hat{\overline{\Omega}}(a_i,p) \right\} \Big|_{r_{D,w}},\tag{10}$$

where  $H_0^{-1}\{\}$  denotes the inverse zeroth-order finite Hankel transform operator,  $r_{D,w} = r_w/B$  is the dimensionless wellbore radius,  $\gamma_{D,s} = \gamma_s T_c, \gamma_s$  is the source well damping coefficient, and

$$\hat{\overline{\Omega}}(a_i, p) = \frac{C_D \left[ 1 - \left\langle \hat{\overline{w}}_D(a_i, p) \right\rangle \right]}{\kappa \eta^2 \xi_w K_1(\xi_w)}.$$
(11)

Malama et al. (2011) showed that

$$\langle \hat{\overline{w}}_{D} \rangle = \frac{1}{\eta b_{D,s}} \frac{\Delta_{0}(d_{D})}{\Delta_{0}(1)} \left\{ \sinh(\eta d_{D}^{*}) - \left[ 2 - \frac{\Delta_{0}(l_{D})}{\Delta_{0}(d_{D})} \right] \sinh(\eta l_{D}^{*}) \right\}, \quad (12)$$

where  $d_D^* = 1 - d_D$ , and  $b_{D,s} = b_s/B$ . According to Butler and Zhan (2004), the source well damping coefficient is  $\gamma_s = 8vL/(L_e r_c^2)$ , where  $\nu$  is the kinematic viscosity of water and L is a characteristic length associated with the perturbed column of water in the source well.

Whereas Malama et al. (2011) used the infinite Hankel transform, here a finite Hankel transform (Sneddon, 1951; Miles, 1971) is used for inversion, with the transform pair defined as

$$\hat{f}(a_i) = \mathsf{H}_0\{f(r_D)\} = \int_0^{R_D} r_D f(r_D) \mathsf{J}_0(r_D a_i) \mathrm{d}r_D,$$

$$f(r_{D}) = \mathsf{H}_{0}^{-1} \left\{ \hat{f}(a_{i}) \right\} = \frac{2}{R_{D}^{2}} \sum_{i=0}^{\infty} \hat{f}(a_{i}) \frac{\mathsf{J}_{0}(r_{D}a_{i})}{\left[\mathsf{J}_{1}(R_{D}a_{i})\right]^{2}}, \tag{13}$$

where  $a_i$  are the roots of  $J_0(R_Da_i) = 0$ ,  $R_D = R/B$ , R is the radius of influence of the source well, and  $J_n()$  is the nth-order first-kind Bessel function (Olver et al., 2010, Section 10.2). For the specified roots

and Hankel transform pair given in (13), a homogeneous Dirichlet boundary condition is enforced at  $r_D = R_D$ . Due to the short duration of the signal, a radius of influence such that  $R \geqslant 2r_{\rm obs}$  is sufficient. The finite Hankel transform is chosen for computational expedience; it is simpler to invert numerically than the infinite Hankel transform (Malama, 2013). Laplace transform inversion is performed using the algorithm of de Hoog et al. (1982). The software used to implement the analytical solution described here is released under an open-source MIT license and is available from a public Bitbucket repository (https://bitbucket.org/klkuhlm/slug-osc).

#### 2.1. Approximation of observation well skin

It is assumed here that the slug test response at the observation well is due to fluid flow through the sub-domains associated with the source and observation wells and the formation shown in Fig. 1. The well skin and formation hydraulic conductivities,  $K_i$ , i=1,2,3, are arranged in series for radial flow, and in parallel for vertical flow. Hence, the effective radial and vertical hydraulic conductivity,  $\langle K_r \rangle$  and  $\langle K_z \rangle$ , of the formation between the source and observation wells are approximated as

$$\langle K_r \rangle = \delta_T / \sum_{n=1}^3 \frac{\delta_i^*}{K_i},$$

and

$$\langle K_z \rangle = \frac{1}{\delta_T} \sum_{n=1}^3 \delta_i K_i,$$

where  $\delta_1^* = (\hat{r}/r_1)\delta_1$  and  $\delta_2^* = (\hat{r}/r_2)\delta_2$ ,  $\delta_T = \sum_{n=1}^3 \delta_i$ ,  $\delta_i$  is the radial thickness of zone  $i, r_1 = (r_w + r_{\rm skin})/2$ ,  $r_2 = (r_{\rm skin} + r_{\rm obs})/2$ , and  $\hat{r} = (r_w + r_{\rm obs})/2$ . This approximate approach follows the work of Shapiro and Hsieh (1998) for using the equivalent hydraulic conductivity approach to account for simple heterogeneity. It is based on the simplifying assumption of a piecewise linear head distribution in the skin and formation. It follows directly from an application of mass conservation and Darcy's law in a radial (cylindrical) flow system. The result may also be obtained using a centered finite difference approximation of the hydraulic gradient at  $r_1$  and  $r_2$  for a head distribution given by Theim equation.

#### 2.2. Observation well storage & inertial effects

The column of water in the observation well oscillates in response to a source well perturbation. It is reasonable to assume that the effective weight of the water column in the observation well controls its head response and damping of the oscillations. Mass balance in the manner of Black and Kipp (1977) and momentum balance (Kipp, 1985; Butler and Zhan, 2004) in the observation well account for wellbore storage and inertial effects. In non-dimensional form, the momentum balance equation is given by

$$\frac{\mathrm{d}^2 s_{D,\mathrm{obs}}}{\mathrm{d} t_D^2} + \gamma_{D,\mathrm{o}} \frac{\mathrm{d} s_{D,\mathrm{obs}}}{\mathrm{d} t_D} + \omega_{D,\mathrm{o}}^2 \ s_{D,\mathrm{obs}} = \omega_{D,\mathrm{o}}^2 \langle s_D \rangle \tag{14}$$

where  $\gamma_{D,o}$  is dimensionless observation well damping coefficient and  $\omega_{D,o}$  is dimensionless observation well characteristic frequency. where  $s_{D,obs}$  is the dimensionless observation well response,  $\langle s_D \rangle$  is the depth-averaged dimensionless formation response across the observation interval. It follows from Butler and Zhan (2004) that  $\gamma_{D,o} = T_c 8 \nu L_{obs} / (L_{e,obs} r_{c,obs}^2)$ ,  $\omega_{D,o} = T_c \sqrt{g/L_{e,obs}}$ , where  $L_{e,obs}$  and  $L_{obs}$  are the characteristic length scales for observation well inertial effects. Here we estimate  $\gamma_o$  and  $\omega_o$  through  $L_{obs}$  and  $L_{e,obs}$  from observation well data. Applying the Laplace transform and solving for  $s_{obs}$  gives

$$\overline{S}_{D,obs} = \overline{\psi_2}(p) \langle \overline{S}_D(r_D, p) \rangle, \tag{15}$$

where  $\overline{\psi}_2(p) = \omega_{D,o}^2 / \left(p^2 + p\gamma_{D,o} + \omega_{D,o}^2\right)$ 

$$\left\langle \hat{\bar{s}}_{D} \right\rangle = \frac{1}{b_{D,o}} \int_{d_{D,o}}^{l_{D,o}} \hat{\bar{s}}_{D}(a_{i}, p, z_{D}) dz_{D}, \tag{16}$$

and  $l_{D,o} = l_o/B$  and  $d_{D,o} = d_o/B$  are the dimensionless depths to the top and bottom of the observation well interval from the watertable. Upon inverting the Laplace transform, one obtains

$$s_{D,\text{obs}} = \int_{0}^{t_D} \psi_2(t_D - \tau) \langle s_D(r_D, \tau) \rangle \, d\tau \tag{17}$$

with  $\psi_2(t) = \mathcal{L}^{-1}\{\overline{\psi}_2(p)\}$ . Eq. (17) is the solution accounting for observation well inertial effects. It is used in the subsequent analysis to estimate hydraulic parameters.

#### 3. Model application to cross-hole slug test data

The model described above is applied to observations collected in a series of multi-level cross-hole pneumatic slug tests performed in June 2013 at the Widen site in north-east Switzerland. The site is on the floodplain of the Thur River, a tributary of the Rhine river (Diem et al., 2010). The multi-well layout of the test site is depicted schematically in Fig. 2(a). The wells used in the experiments are completed in an unconfined sand and gravel aguifer with a saturated thickness of 5.8 m. The aquifer is quaternary post-glacial sediment underlain by an aquitard of low permeability lacustrine sediment comprising fine silt and clay (Diem et al., 2010; Coscia et al., 2011). It is overlain with alluvial loam that constitutes the top soil. The aquifer itself can be further subdivided into a silty sand top layer underlain with silty gravel and a sand layer to a thickness of about 7 m (Diem et al., 2010). The source well is screened across the entire saturated thickness (see Fig. 2(a)). Straddle packers were used to sequentially isolate discrete intervals in the source well. The pressure responses were recorded in three observation wells, which were equipped with a Continuous Multichannel Tubing (CMT) system (Einarson and Cherry, 2002) in which pressure transducers were installed. This system was originally designed for multi-level sampling. It consists of a PVC pipe with seven continuous separate channels or chambers (inner diameter 0.014 m), which are arranged in a honeycomb structure. Each individual chamber has a 0.08 m long slot covered with a sand filter and allows for hydraulic contact with the formation.

#### 3.1. Experimental procedure

The cross-hole pneumatic slug tests were initiated by applying gas pressure to the water column in a chosen interval, then releasing the gas pressure through an outflow valve to provide the instantaneous initial slug perturbation. A double-packer system straddling the test interval ( $b_s=0.35~\mathrm{m}$ ) was used with the pneumatic slug applied through a smaller tubing ( $r_c=1.55\times10^{-2}~\mathrm{m}$ ). The source well used in these tests was well P13, with a wellbore radius of  $r_w=3.15\times10^{-2}~\mathrm{m}$ . The dissipation of the slug was monitored with a pressure transducer in the source well positioned at the top of the water column above the test interval.

The data considered here was obtained in three observations wells labelled MC1, MC2, and MC4 (in Fig. 2(a)) and located at radial distances of 3.9, 2.9, and 2.8 m, respectively, from the source well. The responses at multiple vertical positions in each observation well were monitored with pressure transducers in a seven-channel CMT system with screen intervals of  $b_{\rm o}=8\times10^{-2}$  m. Each channel in the CMT system has an equivalent radius of  $r_{\rm c,o}=6.5\times10^{-3}$  m; installation of a pressure transducer in these

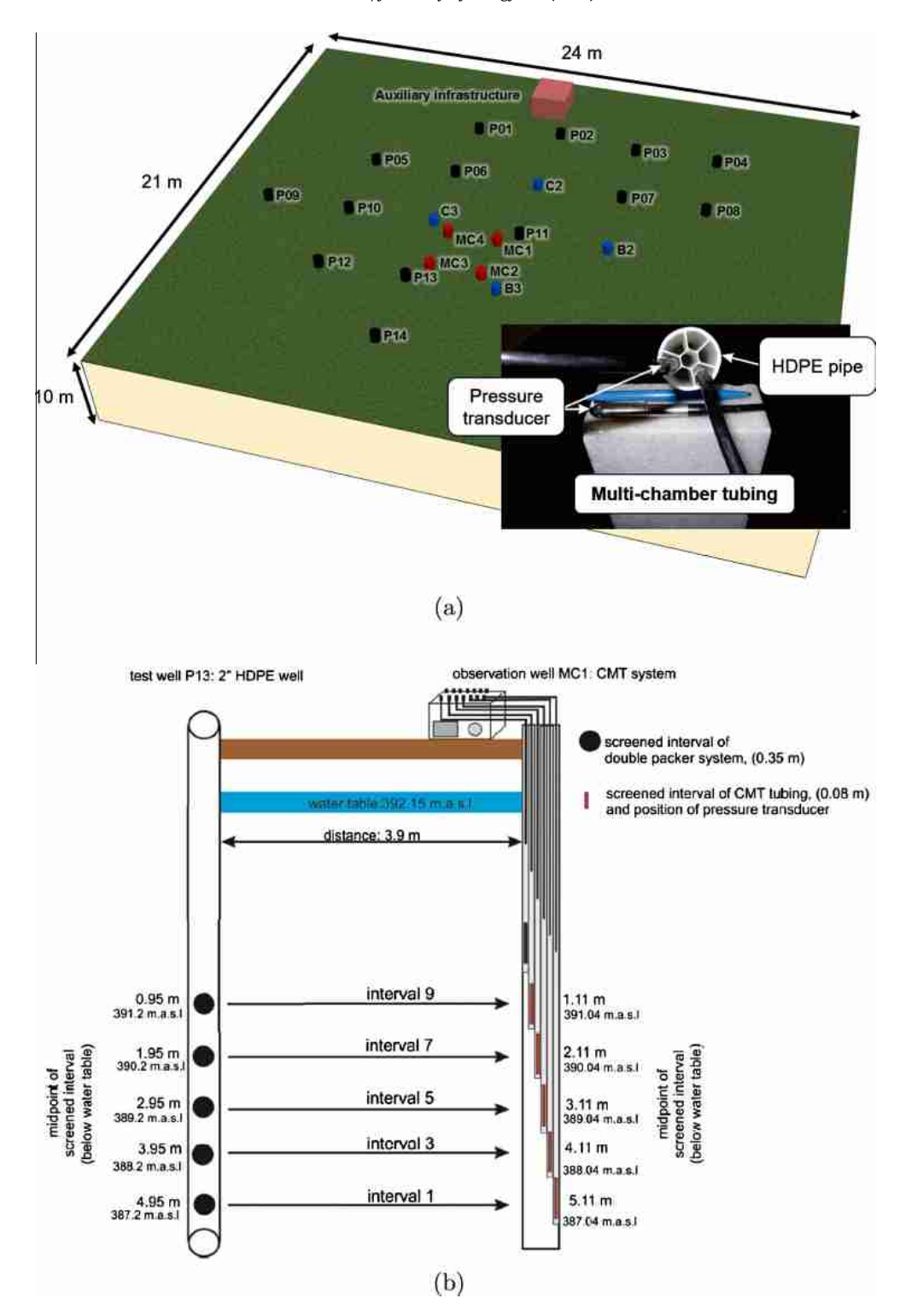


Fig. 2. (a) Multi-well layout and (b) example experimental system setup for cross-hole slug tests at the Widen site, Switzerland. For the example shown, data from interval i is denoted P13-MC1-i

channels reduces their effective radii (and effective wellbore storage) significantly. The CMT system allows for simultaneous monitoring of the response at seven vertical positions for each slug test. Pressure responses were recorded at a frequency of 50 Hz (every 0.02 s) for a period of about 20 s from slug initiation using miniature submersible level transmitters MTM/N 10 manufactured by STS Sensor Technik in Switzerland. The housing diameter of 0.39 in. allowed for pressure measurements in small diameter

(1/2 in.) monitoring wells, stand pipes and bore holes. The stainless steel construction and integral polyurethane cable is ideal for long term installation. The transducer cable is reinforced with Kevlar to avoid elongation in deep boreholes. The experiments reported herein were performed in shallow wells and over a relatively short duration to make cable elongation is negligible.

Only data from the observation intervals at approximately the same vertical position as the source-well test interval are analyzed

here because of their favorable signal-to-noise ratio (SNR). Data from ports not directly in line with the tested interval showed significant decay for the magnitudes of the perturbation used in the field tests. Transducers with greater precision and accuracy or larger source well perturbation are needed to obtain analyzable responses in such ports. A schematic of the experimental setup for tests between wells P13 and MC1 is shown in Fig. 2(b).

#### 3.2. Observation well data

The typical slug test responses observed during tests at the Widen site are shown in Fig. 3. The plots in Fig. 3(a) are the source well responses, and those in (b) are the corresponding responses in an observation well about 3 m radially from the source well. The results clearly show damped oscillations generated in the source well are measurable in an observation well a few meters away. Comparing the results in (a) and (b) also shows the maximum amplitude of the signal decays about two orders of magnitude from the source to the observation well, which decreases the SNR.

The observation well response pairs generally are increasingly damped moving towards the water-table, even when the initial displacements from the equilibrium position are comparable. This is evident in the data from all three profiles shown in Fig. 3, where observation well data collected closer to the water-table appear to be more damped than those at greater depths. Measurable observation well displacements are still obtainable near the water-table (i.e., interval 9 in Fig. 2(b)). The configuration of the equipment made it physically impossible to record the response at the

water-table. Placing a pressure transducer at the water-table would be useful to confirm the appropriate type of boundary condition to represent the water-table. While Malama et al. (2011) and the modified model presented here use the linearized kinematic water-table representation, Hyder et al. (1994) use a constant-head boundary condition to represent the water-table.

#### 3.3. Parameter estimation

The modified model was used to estimate model parameters from data collected in observation wells during the tests at the Widen site. For the present study, to reduce the number of estimated parameters, it is sufficient to assume the aquifer is isotropic  $(K_r = K_z = K)$ , and the skin conductivities of the source and observation wells are equal  $(K_1 = K_3 = K_{\rm skin})$ . Using the non-linear optimization software PEST (Doherty, 2010, 2015), we estimated skin hydraulic conductivity  $(K_{\rm skin})$ , formation hydraulic conductivity (K), specific storage  $(S_s)$ , and the length parameters L and  $L_e$  that characterize the source and observation well damping coefficients and frequencies. It is typical to compute L and  $L_e$  using the formulas (Butler, 2002; Kipp, 1985; Zurbuchen et al., 2002)

$$L = d + \frac{b}{2} \left(\frac{r_c}{r_w}\right)^4,\tag{18}$$

and

$$L_e = L + \frac{b}{2} \left(\frac{r_c}{r_w}\right)^2. \tag{19}$$

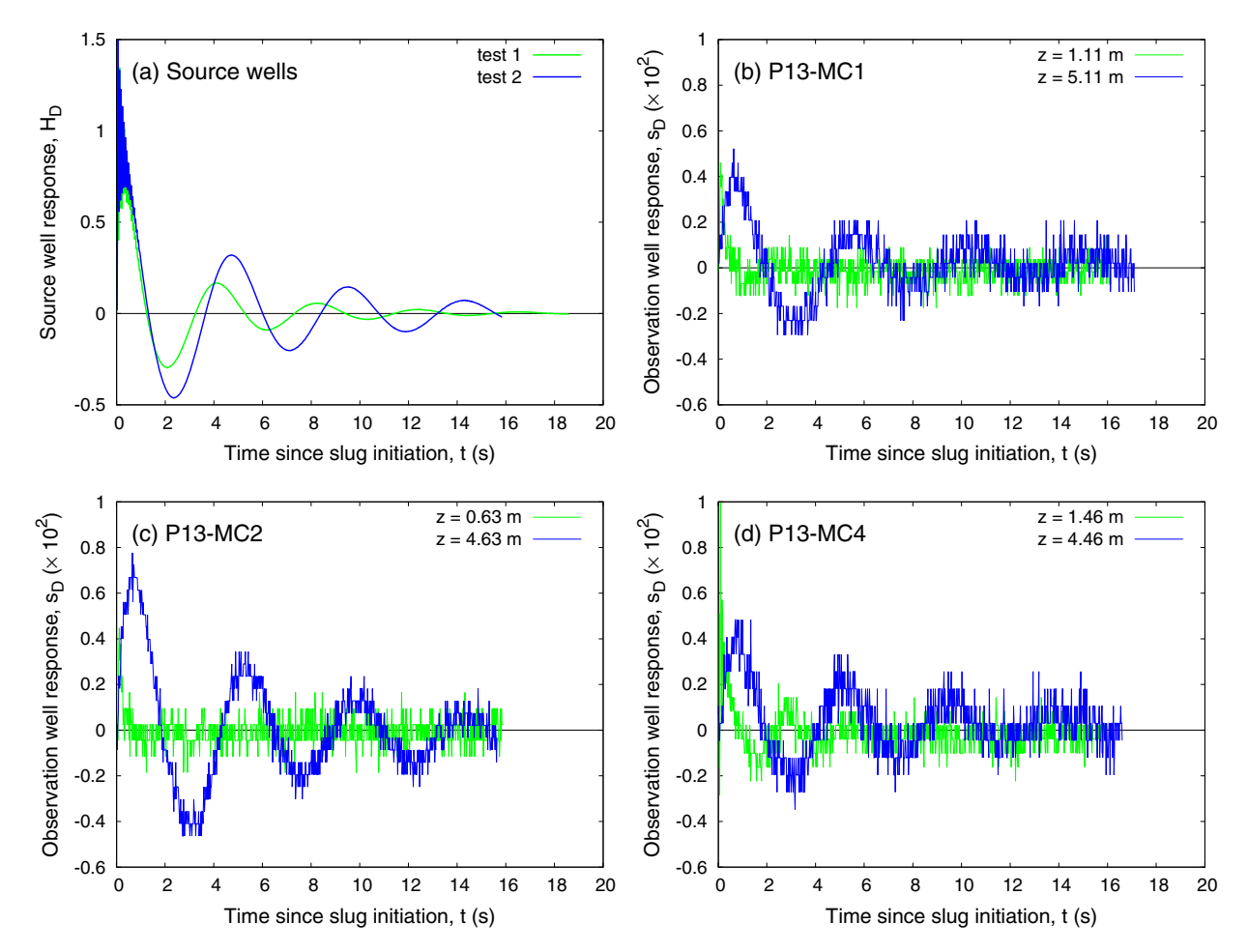


Fig. 3. Typical (a) source and (b-d) observation well responses measured during cross-hole slug tests. Observation well data show increasing damping when approaching the watertable for all three profiles.

The values of L and  $L_e$  computed with these formulas were used as initial guesses during the parameter estimation procedure. The parameters  $L_{e, \rm obs}$  and  $L_{\rm obs}$ , which determine the frequency and damping coefficient of the observation well were also estimated with initial guesses determined similarly. The non-linear optimization software PEST (Doherty, 2010, 2015) was used to estimate the optimal parameters and the model parameter sensitivity at the optimal solution.

The fit of the model to observed cross-hole responses was very sensitive to the time of the initial observation (i.e., the syncing of the clocks at the source and observation wells). Initially it was difficult to get model/data agreement to both early and late-time data without assigning non-physical parameter values. Estimating a modest time shift (off-set) for each test greatly improved model fits to the data. Estimated observation data time delays were between 4 and 6 tenths of a second, which is a permissible time off-set between two synced transducer clocks.

PEST-estimated parameters are summarized in Table 2. A subset of the complete dataset (25% of the 50 Hz data stream) was used in the PEST optimization; this subset is shown in Fig. 4. The corresponding model fits to observation well data are shown in Fig. 4. The relatively large average value of skin conductivity (averaging  $K_{\rm skin} = 8.5 \times 10^{-2} \, {\rm m/s})$  estimated from tests is consistent with a disturbed zone resulting from well installation by directpush. The technology uses a hydraulic hammer supplemented with weight of the direct-push unit to push down drive rods to the desired depth of the projected well. The well casing is then lowered into the drive rods (inner diameter: 0.067 m, outer diameter 0.083 m). By retracting the drive rods, the formation is allowed to collapse back against the casing. The negative skin estimates  $(K_{\text{skin}} \text{ greater than formation } K)$  are indicative of formation collapse due to material bridging resulting in a disturbed zone around the well casing. Skin conductivity estimation variances range from  $10^{-2}$  m<sup>2</sup>/s<sup>2</sup> for low noise data to  $10^3$  m<sup>2</sup>/s<sup>2</sup> noisy data and are indicative of dependence of estimation uncertainties on measurement errors.

Drilling logs and previous hydrogeophysical investigations at the site (Lochbühler et al., 2013; Coscia et al., 2011) indicate a sand and gravel aquifer. The formation hydraulic conductivities estimated here are on the order of  $10^{-4}$ – $10^{-3}$  m/s, and in general agreement with the findings from earlier studies at the site. Coscia et al. (2011) report estimates of the order of  $10^{-3}$ – $10^{-2}$  m/s from multiple pumping and single-well slug tests conducted at the site by Diem et al. (2010). The average values estimated here range from a low of  $7.1 \times 10^{-4}$  m/s to a high value of  $3.8 \times 10^{-3}$  m/s. These and estimates from earlier studies at the site

are reasonable for unconsolidated well-sorted sand and gravel aquifers (Bear, 1972; Fetter, 2001). The vertical variability in the estimates is reflective of site heterogeneity. The objective of multi-level slug tests is to characterize such heterogeneity using a physically based flow model. It should be understood that the model used in this analysis was developed for a homogeneous but anisotropic aquifer. Its application to characterizing heterogeneity is thus limited and only approximate, with data collected at discrete depth intervals assumed to yield hydraulic parameter values associated with that interval. Estimation variances for formation hydraulic conductivity range in magnitude from  $6 \times 10^{-2}$  to  $1.2 \times 10^1$  m<sup>2</sup>/s<sup>2</sup>.

Estimates of specific storage,  $S_s$ , also show only modest variability and are generally of the order of  $10^{-5}$  m<sup>-1</sup>, with the largest value being about  $10^{-5}$  m<sup>-1</sup> and the smallest  $10^{-7}$  m<sup>-1</sup>. The estimated values are indicative of poorly consolidated shallow alluvium, and variability may reflect uncertainty or non-uniqueness in the solution for this configuration and dataset. Estimates of  $S_{\nu}$ were quite variable, with estimation variances of the order of  $10^{-7}$ – $10^2$ . Estimated values of 0.4 correspond to the upper bound during optimization. P13-MC1-1, 7, and 9 resulted in estimated  $S_{\nu}$  values of a few percent, which are physically realistic for these types of sediments and for the linearized kinematic condition at the watertable. In this parameter estimation analysis no significant physical constraints where introduced on the objective function; the observations were allowed to freely constrain the estimates of model parameters. Estimates of the parameter  $L_e$  from data are comparable to those predicted by Eq. (19). However, estimates of L from data are consistently larger than the values predicted by (18).

#### 3.4. Sensitivity analysis

The model sensitivity or Jacobian matrix, **J**, of dimensions  $N \times M$ , where N is the number of observations and M is the number of estimated parameters, is of central importance to parameter estimation. The sensitivity coefficients are simply the elements of the Jacobian matrix; they are the partial derivatives of the model-predicted aquifer head response, s, with respect to the estimated parameter  $\theta_m$ . Sensitivity coefficients are represented here as functions of time using the nomenclature

$$J_{\theta_m}(t) = \frac{\partial s_{D,\text{obs}}}{\partial \theta_m}, \tag{20}$$

where m = 1, 2, ..., M. They describe the sensitivity of predicted model behavior (head response) to the model parameters. They

**Table 2** PEST-estimated model parameters.

Test	$K [m s^{-1}]$	$K_{\rm skin}$ [m s <sup>-1</sup> ]	$S_{\rm s} \ [{\rm m}^{-1}]$	$S_y$ [-]	<i>L</i> [m]	$L_e$ [m]	$L_{\rm obs}$ [m]	$L_{e,obs}$ [m]
P13-MC1-1	$7.81 \times 10^{-4}$	$2.27\times10^{-1}$	$3.39 \times 10^{-5}$	0.037	1.90	5.71	4.07	$1.87 \times 10^{-2}$
P13-MC1-3	$8.85\times10^{-4}$	$1.07\times10^{-1}$	$1.25\times10^{-5}$	0.40	1.18	4.31	2.39	$1.80\times10^{-2}$
P13-MC1-5	$7.70\times10^{-4}$	$2.21\times10^{-1}$	$1.70\times10^{-5}$	0.36	2.53	3.21	3.10	$1.76\times10^{-2}$
P13-MC1-7	$1.28\times10^{-3}$	$1.02\times10^{-2}$	$3.85\times10^{-5}$	0.018	0.23	2.26	11.4	$9.74\times10^{-2}$
P13-MC1-9	$1.48\times10^{-3}$	$6.42\times10^2$	$2.79\times10^{-8}$	0.001	2.95	0.83	8.83	$6.04\times10^{-2}$
P13-MC2-2	$7.67\times10^{-4}$	$1.73\times10^{-1}$	$2.76\times10^{-5}$	0.40	1.07	5.07	3.92	$5.73\times10^{-1}$
P13-MC2-4	$1.36\times10^{-3}$	$2.15\times10^{-1}$	$5.11\times10^{-5}$	0.04	8.01	3.66	4.63	$4.84\times10^{-2}$
P13-MC2-6	$1.08\times10^{-3}$	$6.42\times10^{-2}$	$1.95\times10^{-5}$	0.40	1.38	2.91	2.55	$1.79\times10^{-2}$
P13-MC2-8	$2.22\times10^{-3}$	$4.44\times10^{-1}$	$3.06\times10^{-5}$	0.001	2.26	1.80	5.34	$1.64\times10^{-3}$
P13-MC4-2	$1.60\times10^{-3}$	$3.17\times10^{-1}$	$7.41\times10^{-5}$	0.005	2.39	4.81	6.42	$1.35\times10^{-2}$
P13-MC4-4	$5.27\times10^{-4}$	$3.37\times10^{-1}$	$9.16\times10^{-5}$	0.40	4.56	3.49	9.69	$1.38\times10^{-2}$
P13-MC4-6	$3.79\times10^{-3}$	$2.04\times10^{-2}$	$7.22\times10^{-5}$	0.001	3.24	2.82	3.09	$4.85\times10^{-1}$
P13-MC4-8	$1.46\times10^{-3}$	$6.15\times10^{-2}$	$1.80\times10^{-4}$	0.40	0.78	1.76	9.24	$3.48\times10^{-2}$

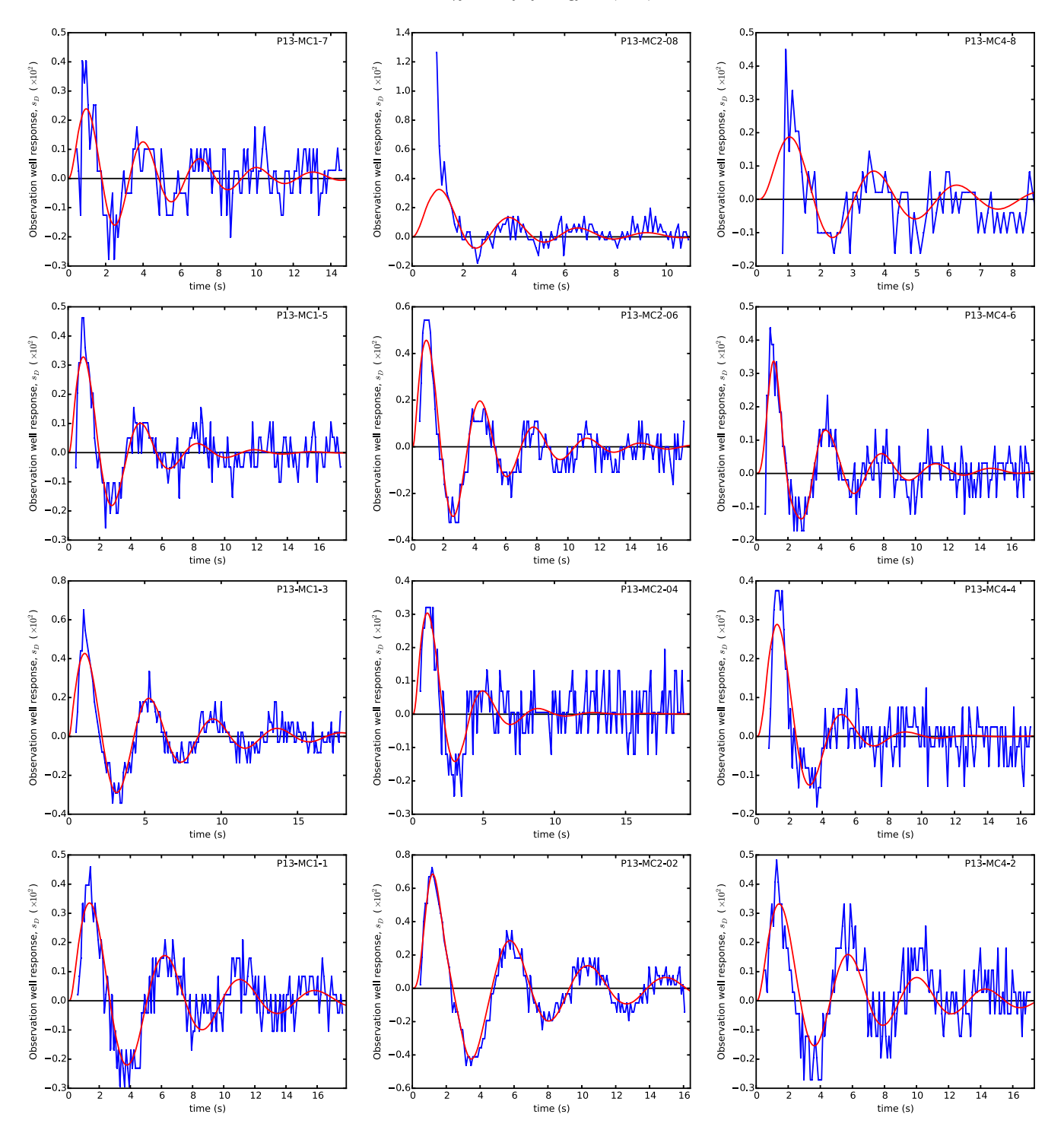


Fig. 4. Model fits to cross-hole slug test data collected along vertical profiles in three observation wells at the Widen Site, Switzerland. The columns correspond to profiles in observation wells 1, 2, and 4.

provide a measure of the ease of estimation (identifiability) of the parameters from system state observations (Jacquez and Greif, 1985). The Jacobian matrix  $\mathbf{J}$  has to satisfy the identifiability condition,  $|\mathbf{J}^T\mathbf{J}| \neq 0$ , for parameters to be estimable. This condition is typically satisfied for linearly independent sensitivity coefficients with appreciably large magnitudes. For this work, the number of parameters estimated is M=8, and the vector of estimated parameters is

$$(\theta_1, \dots, \theta_8) = (K, K_{\text{skin}}, S_s, S_v, L, L_e, L_{\text{obs}}, L_{e, \text{obs}}). \tag{21}$$

Sensitivity coefficients for tests P13-MC1-1 (deepest) and P13-MC1-5 (intermediate depth) are shown as functions of time in Figs. 5 and 6. Semi-log plots of the same information are included to more clearly show the non-zero sensitivity values at late-time.

Generally, the sensitivities are oscillatory functions of time with decaying amplitudes that vary over several orders of magnitude among the parameters. Fig. 5(a) shows the sensitivity to the parameters K,  $K_{\rm skin}$ ,  $S_{\rm s}$ , and  $S_{\rm y}$ . It is clear that well skin conductivity,  $K_{\rm skin}$ , has the highest peak sensitivity at early-time, and is therefore the most easily identifiable parameter from early-time data.

Specific yield,  $S_y$ , has the smallest sensitivities (about an order of magnitude smaller than  $K_{\rm skin}$ ) and was the least identifiable (most difficult to estimate) of all the parameters.

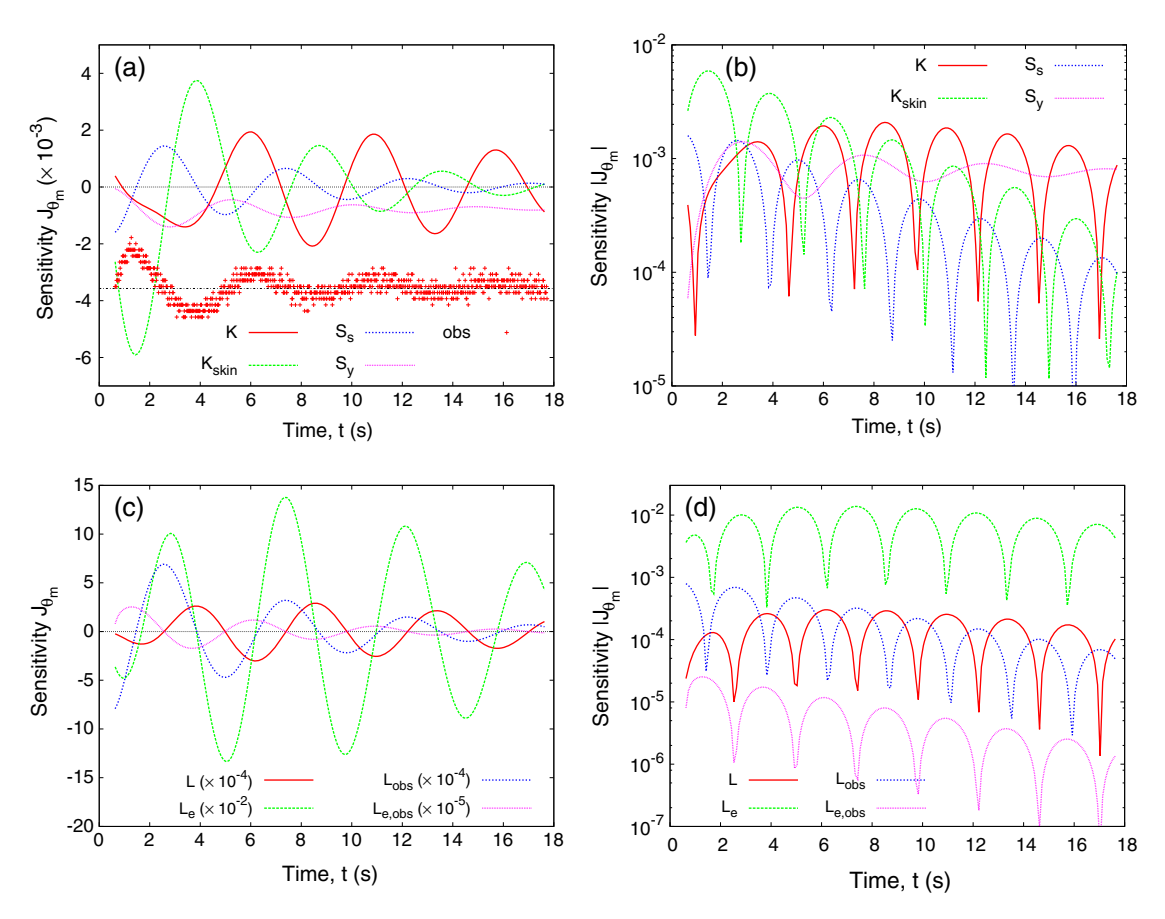
Fig. 5(a) and (b) also shows that the sensitivity functions are generally out of phase with each other as well as with the observed response. For example, the sensitivity function  $J_K(t)$  is almost completely out of phase (phase-shift of  $\sim \pi$ ) with  $J_{K_{\rm skin}}$ . The same is true for  $J_{S_s}(t)$  and  $J_{S_y}(t)$ . This indicates linear-independence of the sensitivity coefficient among all four parameters. This is desirable as it implies that the identifiability condition is satisfied, permitting concomitant estimation of all these four parameters.

Fig. 5(a) shows the  $J_{S_v}$  is oscillatory with the small amplitudes and does not change sign, but decay more slowly than the other sensitivity responses. The predicted model response showed only modest sensitivity to specific yield,  $S_{\nu}$ , but the sensitivity becomes appreciably dominant at late-time (Fig. 5(b)). Malama et al. (2011) showed that slug tests are more sensitive to  $S_v$  at late-time, and for relatively large initial perturbation. At late-time slug test head data are typically of low SNR (diminished data quality) making it difficult to discern effects of specific yield. However, with measurements such as those reported in Malama et al. (2011) for a site in Montana, it is possible to obtain single-well slug tests data with clear effects due to  $S_v$ . The cross-hole slug test data analyzed herein showed only modest watertable effects and the late-time data were not of sufficient quality. This suggests the importance of late-time data to maximize  $S_v$  identifiability and estimability as also noted in Malama et al. (2011).

Fig. 5(c) and (d) shows scaled slug response sensitivities to parameters  $L, L_e, L_{obs}$ , and  $L_{e,obs}$ . They show orders of magnitude of

variability, with sensitivity  $L_e$  being three orders of magnitude larger than sensitivity to  $L_{e, {\rm obs}}$ . Whereas those of the parameters  $L, L_e$ , and  $L_{e, {\rm obs}}$  are linearly independent (not of the same phase), the pair  $L_e$  and  $L_{\rm obs}$  are only linearly independent at very early time; they oscillate with the same phase after about 4 s. This illustrates a long temporal record of observations would not improve the joint estimation of these two parameters.

Fig. 6 shows the same information as depicted in Fig. 5 for a more damped observation location closer to the watertable. Model sensitivity to K is equal to or larger than  $K_{\rm skin}$  for this interval. Sensitivity to  $S_s$  is also higher at early-time. Among parameters  $K, K_{skin}, S_s$ , and  $S_{\nu}$ , sensitivity to  $S_{\nu}$  is the smallest at early time (Fig. 6(b)). The sensitivity to  $S_v$  stays approximately constant with time after the first 10 s of the test, while sensitivities to K,  $K_{skin}$ , and  $S_s$  continue to decrease. It should be noted however, that the unfavorable SNR (low data quality) makes it very difficult to estimate  $S_v$  from late-time data. Collecting data at 3.11 m below the watertable did not yield an appreciable improvement in specific yield identifiability over the interval at 5.11 m depth in Fig. 5. The behavior depicted in Fig. 6 also suggests only data collected in the first 12 s of the test are needed to estimate model parameters at this depth. The sensitivity coefficients for all but K essentially vanish after about 12 s and the identifiability condition is no longer satisfied. Additionally, even for the case where the sensitivity coefficients appear to be in phase (linearly dependent) at early-time (compare  $J_K(t)$  and  $J_{K_{\rm skin}}(t)$  for  $t\leqslant 2$  s for test P13-MC1-5), they quickly (in the first 12 s) become linearly independent with time. This again indicates that a temporal record of the response longer than a few seconds is sufficient for joint estimation of these two parameters.



**Fig. 5.** Temporal variation of the sensitivity coefficients (linear scale (a and c) and log scale (b and d)) for the indicated parameters at the source-observation pair P13-MC1-1 (5.1 m below watertable). Subplot (a) shows observed response.

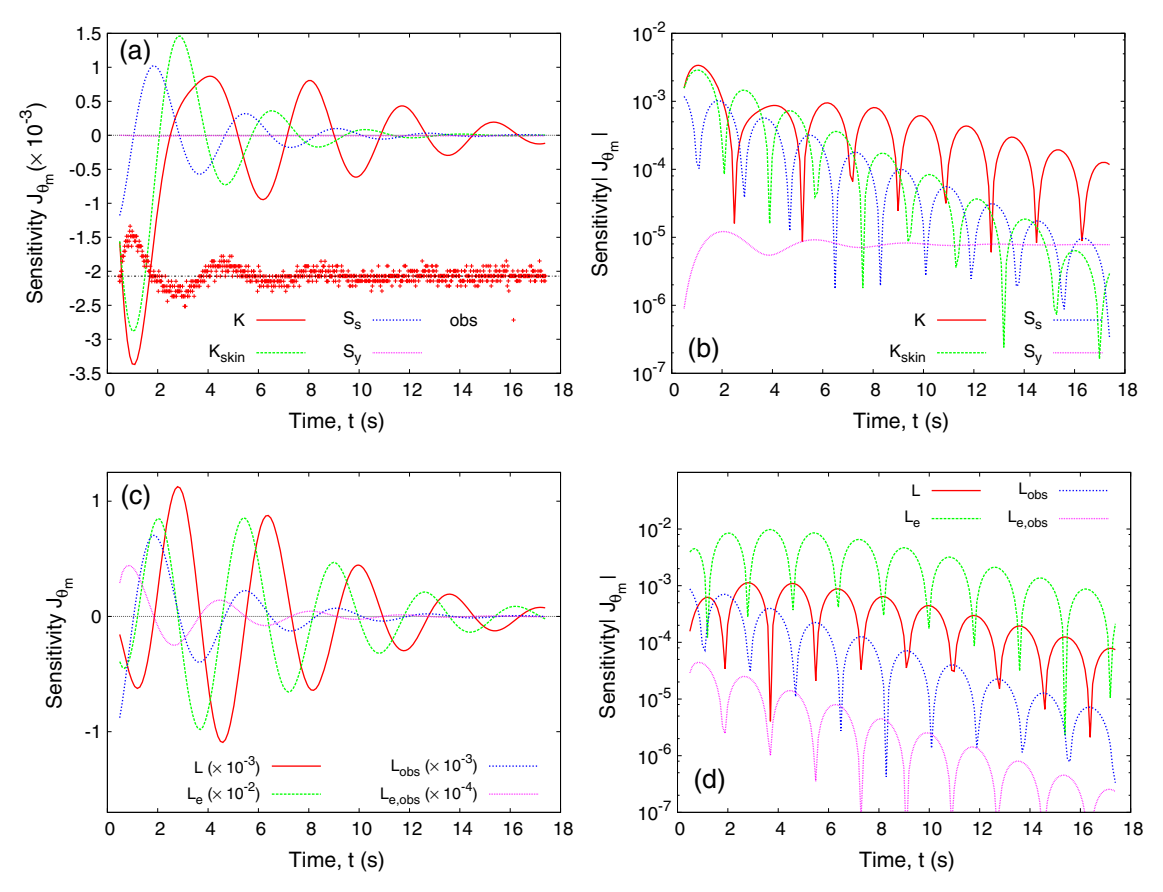


Fig. 6. Temporal variation of the sensitivity coefficients (linear scale (a and c) and log scale (b and d)) for the indicated parameters at the source-observation pair P13-MC1-5 (3.1 m below watertable). Subplot (a) shows observed response (same scale as response in Fig. 5).

### 4. Conclusions

Cross-hole slug test data were analyzed with an extended version of the model of Malama et al. (2011). The semi-analytical model was modified for:

- 1. predicting heads at observation wells,
- 2. inclusion of borehole skin effects,
- 3. use of the finite Hankel transform for computation expediency, and
- 4. inclusion of observation well storage and inertial effects.

Estimates were obtained of formation and source/observation well skin hydraulic conductivity, specific storage, specific yield, and well characteristics that control oscillation frequency and degree of damping. The aim of the study was to evaluate the use of cross-hole slug test data to characterize vertical unconfined aguifer heterogeneity and understand identifiability and estimability of these parameters, especially specific yield. Estimated values of hydraulic conductivity and specific storage from PEST are indicative of a heterogeneous sand and gravel aquifer. Parameter estimation and sensitivity analysis show the model has effectively linearly independent sensitivity coefficients with respect to seven of the eight parameters estimated. These parameters are clearly jointly estimable from the data over the duration of the tests. It should be understood that the model used in this analysis was developed for a homogeneous but anisotropic aquifer and is thus of only limited and approximate applicability to analysis of a heterogeneous system.

Of the parameters estimated, model predictions were least sensitive to specific yield even near the watertable, which implies it was the least identifiable parameter. This is due to a combination of factors, including

- 1. the short duration of the data record due to rapid signal decay with time (<20 s);
- the increasing damping observed in monitoring locations near the watertable (resulting in even shorter temporal records), and:
- 3. the decreasing signal strength near the watertable, resulting in a lower signal-to-noise.

The sensitivity function with respect to specific yield shows a relatively modest increase in magnitude with time (model sensitivity to the other model parameters tends to decrease, while that of  $S_y$  asymptotically tends to a non-zero constant value), suggesting the importance of late-time data to improve its estimation. The analysis of Malama et al. (2011) also indicated that the largest effect of specific yield on slug test response is at late-time, at which time the amplitude of the signal has decayed significantly in magnitude and quality. The absence of good quality late-time observations and the relative low sensitivities of specific yield explain the wide variability of the estimates of  $S_v$ .

An important shortcoming of using cross-hole slug tests to characterize heterogeneity, as has been suggested in several field (Brauchler et al., 2010, 2011) and synthetic (Paradis et al., 2015) hydraulic tomography studies, is the significant decay of the signal with distance from the source well and close to the water-table.

These lead to low quality observations with low signal-to-noise ratios (SNR), and would require test redesign to improve parameter identifiability and estimability. One approach to change test design is to conduct tests with a sufficiently large initial displacement in the source well to achieve favorable SNR at late-time in the observation wells. This may, however, introduce non-linearities and potentially increase the importance of unsaturated flow above the watertable (Mishra and Neuman, 2011). Another approach is to use more sensitive and low-noise pressure sensors, which would increase costs significantly, especially in the cross-hole multilevel testing set-up where a large network of sensors is used for data acquisition. This would be particularly useful close to the watertable and further from the source well due to significant signal strength decay decline. This decline in signal strength limits the usefulness of crosshole slug tests for large-scale aquifer characterization using hydraulic tomography. Lastly, conducting multiple test repetitions and stacking the response data, akin to seismic data stacking (Jones and Levy, 1987), can be used to amplify signal and increase the SNR.

#### Acknowledgements

Sandia National Laboratories is a multi-program laboratory managed and operated by Sandia Corporation, a wholly owned subsidiary of Lockheed Martin Corporation, for the U.S. Department of Energy's National Nuclear Security Administration under contract DE-AC04-94AL85000.

We are grateful to Dr. Walter Illman and the anonymous reviewer for their insightful comments and suggestions.

# Appendix A. Solution with linearized watertable kinematic condition

The solution can be written in dimensionless form for the intervals above, below, and across from the source well completion interval as

$$s_{D} = \begin{cases} s_{D}^{(1)} & \forall z_{D} \in [0, d_{D}] \\ s_{D}^{(2)} & \forall z_{D} \in [d_{D}, l_{D}] \\ s_{D}^{(3)} & \forall z_{D} \in [l_{D}, 1], \end{cases}$$
(A.1)

where  $s_D^{(n)}$  solves

$$\frac{\partial s_D^{(n)}}{\partial t_D} = \frac{1}{r} \frac{\partial}{\partial r_D} \left( r_D \frac{\partial s_D^{(n)}}{\partial r_D} \right) + \kappa \frac{\partial^2 s_D^{(n)}}{\partial z_D^2}. \tag{A.2}$$

The initial and boundary conditions are

$$s_D^{(n)}(t_D=0) = s_D^{(n)}(r_D=R_D) = 0$$
 (A.3)

$$\underset{r_{D}\rightarrow0}{\lim}r_{D}\frac{\partial s_{D}^{(1)}}{\partial r_{D}}=\underset{r_{D}\rightarrow0}{\lim}r_{D}\frac{\partial s_{D}^{(3)}}{\partial r_{D}}=0 \tag{A.4}$$

$$\frac{\partial s_D^{(1)}}{\partial z_D}\bigg|_{z_D=0} = \frac{1}{\alpha_D} \frac{\partial s_D^{(1)}}{\partial t_D}\bigg|_{z_D=0} \tag{A.5}$$

$$\left. \frac{\partial s_D^{(3)}}{\partial z_D} \right|_{z_D = 1} = 0 \tag{A.6}$$

$$r_D \frac{\partial s_D^{(2)}}{\partial r_D} \bigg|_{r_D = r_{D,u}} = C_D \frac{\mathrm{d}\Phi_{\mathrm{uc}}}{\mathrm{d}t_D},\tag{A.7}$$

$$\Phi_{\rm uc}(t_D=0)=1,\tag{A.8}$$

and

$$\beta_2 \frac{\mathrm{d}^2 \Phi_{\mathrm{uc}}}{\mathrm{d}t_D^2} + \beta_1 \frac{\mathrm{d}\Phi_{\mathrm{uc}}}{\mathrm{d}t_D} + \Phi_{\mathrm{uc}} = \frac{1}{b_D} \int_{d_D}^{l_D} s_D^{(2)}(r_{D,w}, z_D, t_D) \, \mathrm{d}z_D. \tag{A.9}$$

Additionally, continuity of head and flux is imposed at  $z_D=d_D$  and  $z_D=l_D$  via

$$s_D^{(1)}(t_D, r_D, z_D = d_D) = s_D^{(2)}(z_D = d_D),$$
 (A.10)

$$\left. \frac{\partial s_D^{(1)}}{\partial z_D} \right|_{z_D = d_D} = \left. \frac{\partial s_D^{(2)}}{\partial z_D} \right|_{z_D = d_D},\tag{A.11}$$

$$s_D^{(3)}(t_D, r_D, z_D = l_D) = s_D^{(2)}(z_D = l_D), \tag{A.12}$$

and

$$\left. \frac{\partial s_D^{(3)}}{\partial z_D} \right|_{z_D = l_D} = \left. \frac{\partial s_D^{(2)}}{\partial z_D} \right|_{z_D = l_D}. \tag{A.13}$$

This flow problem is solved using Laplace and Hankel transforms. Taking the Laplace and Hankel transforms of Eq. (A.2) for n=1,3, and taking into account the initial and boundary conditions in (A.3) and (A.4), gives the ordinary differential equation

$$\frac{d^2 \widehat{\bar{s}}_D^{(n)}}{dz_D^2} - \eta^2 \widehat{\bar{s}}_D^{(n)} = 0 \tag{A.14}$$

where  $\hat{\mathbf{s}}_D^{(n)} = \mathsf{H} \Big\{ \mathcal{L} \Big\{ \mathbf{s}_D^{(n)} \Big\} \Big\}$  is the double Laplace-Hankel transform of the function  $\mathbf{s}_D^{(n)}, \eta^2 = (p+a_i^2)/\kappa$ , and p and  $a_i$  are the Laplace and finite Hankel transform parameters, respectively. Eq. (A.14) has the general solution

$$\hat{S}_{D}^{(n)} = A_n e^{\eta z_D} + B_n e^{-\eta z_D}. \tag{A.15}$$

The boundary condition at the watertable, Eq. (A.16), in Laplace-Hankel transform space, becomes

$$\frac{\left. \frac{\partial \widehat{S}_D^{(1)}}{\partial z_D} \right|_{z_D = 0}}{\left. \frac{p}{\alpha_D} \widehat{S}_D^{(1)}(z_D = 0). \right. \tag{A.16}$$

Applying this boundary condition leads to

$$(1-\varepsilon)A_1 - (1+\varepsilon)B_1 = 0, \tag{A.17}$$

where  $\varepsilon=p/(\eta\alpha_D)$ . Applying the continuity conditions at  $z_D=d_D$  (Eqs. (A.10) and (A.11)), lead to

$$A_1 e^{\eta d_D} + B_1 e^{-\eta d_D} = \hat{\bar{s}}_D^{(2)}(z_D = d_D),$$
 (A.18)

and

$$\eta \left( A_1 e^{\eta d_D} - B_1 e^{-\eta d_D} \right) = \frac{d\hat{\overline{s}}_D^{(2)}}{dz_D} \bigg|_{z_D = d_D}. \tag{A.19}$$

Similarly, applying the no flow boundary condition at  $z_D = 1$  (Eq. (A.6)), leads to

$$\hat{\bar{s}}_{D}^{(3)} = 2B_3 e^{-\eta} \cosh\left(\eta z_{D}^*\right),\tag{A.20}$$

where  $z_D^* = 1 - z_D$ . Continuity conditions at  $z_D = l_D$  lead to

$$2B_3 e^{-\eta} \cosh(\eta l_D^*) = \hat{\bar{s}}_D^{(2)}(z_D = l_D), \tag{A.21}$$

$$-2\eta B_3 e^{-\eta} \sinh(\eta l_D^*) = \frac{d\hat{s}_D^{(2)}}{dz_D}\bigg|_{z_0 = l_D}, \tag{A.22}$$

where  $l_D^* = 1 - l_D$  and  $d_D^* = 1 - d_D$ . For n = 2, solving Eq. (A.2) in Laplace-Hankel transform space yields

$$\hat{\mathbf{S}}_{\mathsf{D}}^{(2)} = \hat{\overline{\mathbf{u}}}_{\mathsf{D}} + \hat{\overline{\mathbf{v}}}_{\mathsf{D}},\tag{A.23}$$

where

$$\hat{\overline{u}}_D = \frac{C_D(1 - p\overline{\Phi}_{uc})}{\kappa \eta^2 \xi_w K_1(\xi_w)}, \tag{A.24}$$

and

$$\hat{\overline{\nu}}_D = A_2 e^{\eta z_D} + B_2 e^{-\eta z_D}. \tag{A.25}$$

The five Eqs. (A-17)–(A-19), (A-21) and (A-22), together with Eq. (A.23) can be used to determine the five unknown coefficients  $A_1$ ,  $A_2$ , and  $B_1$ – $B_3$ . It can then be shown that

$$\hat{\overline{v}}_{D} = -\frac{\hat{\overline{u}}_{D}}{A_{0}} \left\{ A_{1} \cosh \left( \eta z_{D}^{*} \right) + \sinh \left( \eta_{D}^{*} \right) \left[ \cosh \left( \eta z_{D} \right) + \epsilon \sinh \left( \eta z_{D} \right) \right] \right\}. \tag{A.26}$$

The integral in Eq. (A.9) is

$$\frac{1}{b_D}\int_{d_D}^{l_D}\hat{\overline{s}}_D^{(2)}\,dz_D=\hat{\overline{u}}_D+\frac{1}{b_D}\int_{d_D}^{l_D}\hat{\overline{v}}_D\,dz_D=\hat{\overline{u}}_D+\left\langle\hat{\overline{v}}_D\right\rangle. \tag{A.27}$$

Substituting Eq. (A.26) into (A.27) leads to

$$\frac{1}{b_D} \int_{d_D}^{l_D} \hat{\overline{s}}_D^{(2)} dz_D = \hat{\overline{u}}_D \left( 1 - \left\langle \hat{\overline{w}}_D \right\rangle \right), \tag{A.28}$$

where

$$\begin{split} &\langle \hat{\overline{w}}_{D} \rangle = \frac{1}{b_{D} \eta \Delta_{0}} \big[ \Delta_{1} \sinh \big( \eta d_{D}^{*} \big) + (\Delta_{2} - 2 \Delta_{1}) \sinh \big( \eta l_{D}^{*} \big) \big], \\ &\Delta_{0} = \sinh(\eta) + \varepsilon \cosh(\eta), \\ &\Delta_{1} = \sinh(\eta d_{D}) + \varepsilon \cosh(\eta d_{D}), \\ &\Delta_{2} = \sinh(\eta l_{D}) + \varepsilon \cosh(\eta l_{D}). \end{split} \tag{A.29}$$

Taking the Laplace transform of (A.9) and replacing the integral on the left-hand-side with (A.28), gives

$$(p^2 + \beta_1 p + \beta_2)\overline{\Phi}_{uc} - p - \beta_1 = \frac{1}{2} (1 - p\overline{\Phi}_{uc})\overline{\Omega}$$
 (A.30)

where  $\widehat{\Omega}$  is defined in (11). Solving (A.30) for  $\overline{\Phi}_{uc}$  yields the required source well response in Laplace space.

#### Appendix B. Supplementary material

Supplementary data associated with this article can be found, in the online version, at http://dx.doi.org/10.1016/j.jhydrol.2016.06.060.

### References

- Audouin, O., Bodin, J., 2008. Cross-borehole slug test analysis in a fractured limestone aquifer. J. Hydrol. 348 (3), 510–523.
- Barker, J.A., Black, J.H., 1983. Slug tests in fissured aquifers. Water Resour. Res. 19 (6), 1558–1564.
- Bear, J., 1972. Dynamics of Fluids in Porous Media. Dover Publications, Inc., New York.
- Beckie, R., Harvey, C.F., 2002. What does a slug test measure: an investigation of instrument response and the effects of heterogeneity. Water Resour. Res. 38 (12), 26-1-26-14.
- Belitz, K., Dripps, W., 1999. Cross-well slug testing in unconfined aquifers: a case study from the Sleepers River watershed, Vermont. Ground Water 37 (3), 438– 447
- Black, J.H., Kipp Jr., K.L., 1977. Observation well response time and its effect upon aquifer tests. J. Hydrol. 34, 297–306.
- Bouwer, H., Rice, R., 1976. A slug test for determining hydraulic conductivity of unconfined aquifers with completely or partially penetrating wells. Water Resour. Res. 12 (3), 423–428.
- Brauchler, R., Hu, R., Dietrich, P., Sauter, M., 2011. A field assessment of highresolution aquifer characterization based on hydraulic travel time and hydraulic attenuation tomography. Water Resour. Res. 47 (3).
- Brauchler, R., Hu, R., Vogt, T., Al-Halbouni, D., Heinrichs, T., Ptak, T., Sauter, M., 2010. Cross-well slug interference tests: an effective characterization method for resolving aquifer heterogeneity. J. Hydrol. 384 (1–2), 33–45.
- Bredehoeft, J.D., Papadopulos, I.S., 1980. A method for determining the hydraulic properties of tight formations. Water Resour. Res. 16 (1), 233–238.

- Butler Jr., J.J., 1998. The Design, Performance, and Analysis of Slug Tests. Lewis Publishers, Boca Raton.
- Butler Jr., J.J., 2002. A simple correction for slug tests in small-diameter wells. Ground Water 40 (3), 303–307.
- Butler Jr., J.J., 2005. Hydrogeological methods for estimation of spatial variations in hydraulic conductivity. In: Hydrogeophysics. Springer, pp. 23–58.
- Butler Jr., J.J., Zhan, X., 2004. Hydraulic tests in highly permeable aquifers. Water Resour. Res. 20, W12402.
- Cooper, H.H.J., Bredehoeft, J.D., Papadopulos, I.S., 1967. Response of a finite-diameter well to an instantaneous charge of water. Water Resour. Res. 3 (1), 263–269.
- Coscia, I., Greenhalgh, S.A., Linde, N., Doetsch, J., Marescot, L., Günther, T., Vogt, T., Green, A.G., 2011. 3D crosshole ERT for aquifer characterization and monitoring of infiltrating river water. Geophysics 76 (2), G49–G59.
- de Hoog, F.R., Knight, J.H., Stokes, A.N., 1982. An improved method for numerical inversion of Laplace transforms. SIAM J. Sci. Stat. Comput. 3 (3), 357–366.
- Diem, S., Vogt, T., Höhn, E., 2010. Spatial characterization of hydraulic conductivity of perialpine alluvial gravel-and-sand aquifers: A comparison of methods. Grundwasser 15, 241–251 (in German).
- Doherty, J., 2010. PEST User-Manual: Model-independent Parameter Estimation. fifth ed. Watermark Numerical Computing, Australia.
- Doherty, J., 2015. Calibration and Uncertainty Analysis for Complex Environmental Models. Watermark Numerical Computing, Brisbane, Australia.
- Einarson, M.D., Cherry, J.A., 2002. A new multilevel ground water monitoring system using multichannel tubing. Groundwater Monit. Remed. 22 (4), 52–65. Fetter, C.W., 2001. Applied Hydrogeology, third ed. Prentice Hall.
- Hyder, Z., Butler Jr., J.J., McElwee, C.D., Liu, W., 1994. Slug tests in partially penetrating wells. Water Resour. Res. 30 (11), 2945–2957.
- Illman, W.A., Liu, X., Takeuchi, S., Yeh, T.-C.J., Ando, K., Saegusa, H., 2009. Hydraulic tomography in fractured granite: Mizunami underground research site, japan. Water Resour. Res. 45 (1).
- Illman, W.A., Neuman, S.P., 2001. Type curve interpretation of a cross-hole pneumatic injection test in unsaturated fractured tuff. Water Resour. Res. 37 (3), 583–603.
- Jacquez, J.A., Greif, P., 1985. Numerical parameter identifiability and estimability: integrating identifiability, estimability, and optimal sampling design. Math. Biosci. 77 (1), 201–227.
- Ji, S.-H., Koh, Y.-K., 2015. Nonlinear groundwater flow during a slug test in fractured rock. J. Hydrol. 520, 30–36.
- Jones, I.F., Levy, S., 1987. Signal-to-noise ratio enhancement in multichannel seismic data via the Karhunen-Loéve transform. Geophys. Prospect. 35 (1), 12–32.
- Kipp Jr., K.L., 1985. Type curve analysis of inertial effects in the response of a well to a slug test. Water Resour. Res. 21 (9), 1397–1408.
- Lochbühler, T., Doetsch, J., Brauchler, R., Linde, N., 2013. Structure-coupled joint inversion of geophysical and hydrological data. Geophysics 78 (3), ID1-ID14.
- Malama, B., 2013. Advances in Hydrogeology. Springer (Chapter Measurement of Streaming Potentials Generated During Laboratory Simulations of Unconfined Pumping Tests).
- Malama, B., Kuhlman, K.L., Barrash, W., Cardiff, M., Thoma, M., 2011. Modeling slug tests in unconfined aquifers taking into account water table kinematics, wellbore skin and inertial effects. J. Hydrol. 408 (1–2), 113–126.
- Miles, I.W., 1971. Integral Transforms in Applied Mathematics. Cambridge.
- Mishra, P.K., Neuman, S.P., 2011. Saturated-unsaturated flow to a well with storage in a compressible unconfined aquifer. Water Resour. Res. 47 (5).
- Neuman, S.P., 1972. Theory of flow in unconfined aquifers considering delayed response of the water table. Water Resour. Res. 8 (4), 1031–1045.
- Olver, F.W.J., Lozier, D.W., Boisvert, R.F., Clark, C.W. (Eds.), 2010. NIST Handbook of Mathematical Functions. Cambridge University Press, New York, NY (print companion to DLMF (2014)).
- Ostendorf, D.W., Lukas, W.G., Hinlein, E.S., 2015. Closed form flow model of a damped slug test in a fractured bedrock borehole. J. Hydrol. 529, 1116–1128.
- Paradis, D., Gloaguen, E., Lefebvre, R., Giroux, B., 2015. Resolution analysis of tomographic slug test head data: two-dimensional radial case. Water Resour. Res. 51 (4), 2356–2376.
- Paradis, D., Lefebvre, R., 2013. Single-well interference slug tests to assess the vertical hydraulic conductivity of unconsolidated aquifers. J. Hydrol. 478, 102– 118
- Paradis, D., Tremblay, L., Lefebvre, R., Gloaguen, E., Rivera, A., Parent, M., Ballard, J.-M., Michaud, Y., Brunet, P., 2014. Field characterization and data integration to define the hydraulic heterogeneity of a shallow granular aquifer at a subwatershed scale. Environ. Earth Sci. 72 (5), 1325–1348.
- Quinn, P.M., Parker, B.L., Cherry, J.A., 2013. Validation of non-Darcian flow effects in slug tests conducted in fractured rock boreholes. J. Hydrol. 486, 505–518.
- Shapiro, A.M., Hsieh, P.A., 1998. How good are estimates of transmissivity from slug tests in fractured rock? Groundwater 36 (1), 37–48.
- Sneddon, I.N., 1951. Fourier Transforms. McGraw-Hill.
- Spane, F., 1996. Applicability of slug interference tests for hydraulic characterization of unconfined aquifers:(1) analytical assessment. Ground Water 34 (1), 66–74.
- Spane, F., Thorne, P., Swanson, L., 1996. Applicability of slug interference tests for hydraulic characterization of unconfined aquifers:(2) field test examples. Ground Water 34 (5), 925–933.
- Ground Water 34 (5), 925–933.

  Springer, R.K., Gelhar, L.W., 1991. Characterization of Large-scale Aquifer Heterogeneity in Glacial Outwash by Analysis of Slug Tests with Oscillatory Response. Cape Cod, Massachusetts. Water Resources Investigations Report 91-4034, U.S. Geological Survey.

- Vesselinov, V.V., Neuman, S.P., Illman, W.A., 2001. Three-dimensional numerical inversion of pneumatic cross-hole tests in unsaturated fractured tuff: 2. Equivalent parameters, high-resolution stochastic imaging and scale effects. Water Resour. Res. 37 (12), 3019–3041.

  Wang, Q., Zhan, H., Wang, Y., 2015. Non-Darcian effect on slug test in a leaky confined aquifer. J. Hydrol. 527, 747–753.

  Yeh, T.-C.J., Liu, S., 2000. Hydraulic tomography: development of a new aquifer test method. Water Resour. Res. 36 (8), 2005–2105.
- method. Water Resour. Res. 36 (8), 2095-2105.
- Zlotnik, V.A., McGuire, V.L., 1998. Multi-level slug tests in highly permeable formations: 1. Modifications of the Springer-Gelhar (SG) model. J. Hydrol. 204 (1), 271–282.
- Zurbuchen, B.R., Zlotnik, V.A., Butler Jr., J.J., 2002. Dynamic interpretation of slug tests in highly permeable aquifers. Water Resour. Res. 38 (3), 1025. http://dx.doi.org/10.1016/j.jhydrol.2007.08.018.